

Article

Two-Stage Evolution of the Altyn Tagh Fault System during the Tertiary: Constraints from Heavy Mineral Chemistry in Sediments of the Northwestern Qaidam Basin, Western China

Lu Bai ¹, Ling Fu ², Ping Guan ^{1,*} and Daowei Zhang ³

¹ Ministry of Education Key Laboratory of Orogenic Belts and Crustal Evolution, School of Earth and Space Sciences, Peking University, Beijing 100871, China; bailu268@126.com

² Research Institute of Petroleum Exploration and Development (RIPED), PetroChina, Beijing 100083, China; fuling@petrochina.com.cn

³ Previously in Research Institute of Exploration and Development, Qinghai Oilfield Company, PetroChina, Dunhuang 736202, China; zdwqh@petrochina.com.cn

* Correspondence: pguan@pku.edu.cn

Abstract: The tectonic evolution of the Altyn Tagh Fault (ATF) remains controversial during the Tertiary. Qaidam Basin is the largest and highest plateau inland basin inside the Tibet Plateau. Sediments in the basin provide sedimentary records of the evolution history of its surrounding orogens, such as the ATF, located on the northwest margin of the Qaidam Basin. Comprehensive analyses of sandstone petrography, heavy mineral assemblages, and mineral geochemistry were adopted to effectively indicate the tectonic evolution history of ATF. The result indicates that the sediments in a wide range of the northwestern Qaidam Basin (e.g., the Xichagou section, the Yueyashan section) were derived from the Altyn Mountains. The increasing immaturity of sediments, increased denudation, and sedimentation processes from the early-middle Miocene to the Pliocene can be explained by the active tectonic setting of the ATF. During the early Miocene (ca. 22 Ma), there was an abrupt change in the heavy mineral composition of sediments in the northwestern Qaidam Basin. This change may be attributed to the large-scale slip motion along the ATF. Therefore, ~22 Ma is the key transforming period of the ATF system. On the foundation of the above, we suggest a two-stage evolution model of the ATF during the Tertiary: (1) From the late Eocene to the Oligocene, the tectonic setting of the ATF was relatively calm; (2) During the early Miocene period, the ATF underwent large-scale tectonic activation. It is likely to be a strike-slip tectonic activity, accompanied by an uplift of the Altyn Mountains. The active tectonic setting of the ATF was sustained after the Miocene.

Keywords: Altyn Tagh Fault; Altyn Mountains; Qaidam Basin; provenance analysis; tectonic evolution history



Citation: Bai, L.; Fu, L.; Guan, P.; Zhang, D. Two-Stage Evolution of the Altyn Tagh Fault System during the Tertiary: Constraints from Heavy Mineral Chemistry in Sediments of the Northwestern Qaidam Basin, Western China. *Minerals* **2023**, *13*, 1076. <https://doi.org/10.3390/min13081076>

Academic Editors: Georgia Pe-Piper, Yonghong Shi, Fukun Chen and Jiahao Li

Received: 5 June 2023

Revised: 9 August 2023

Accepted: 11 August 2023

Published: 13 August 2023



Copyright: © 2023 by the authors. Licensee MDPI, Basel, Switzerland. This article is an open access article distributed under the terms and conditions of the Creative Commons Attribution (CC BY) license (<https://creativecommons.org/licenses/by/4.0/>).

1. Introduction

The activities of the Altyn Tagh Fault (ATF) and Altyn Mountains have an intimate relationship in genesis [1,2]. The ~1600 km-long active ATF is located on the northern edge of the Tibetan plateau and defines the northwestern edge of the Qaidam Basin (Figure 1a,b) [3–5]. The tectonic evolution of the ATF controls the development of the northwestern margin of the Qaidam Basin and figures prominently in constraining the formation and mechanism of the Tibetan plateau [6]. Thus, the geological study of the ATF system (especially its tectonic history) attracts many scholars all over the world. After decades of intensive investigation, the ATF is considered a left-lateral strike-slip fault that has undergone multiple stages of activities during the Tertiary [7–10]. However, a great deal of controversy still exists about its Tertiary evolution, and the key issue is the initial time of strike-slip movement on the fault [1,5–7,11,12].

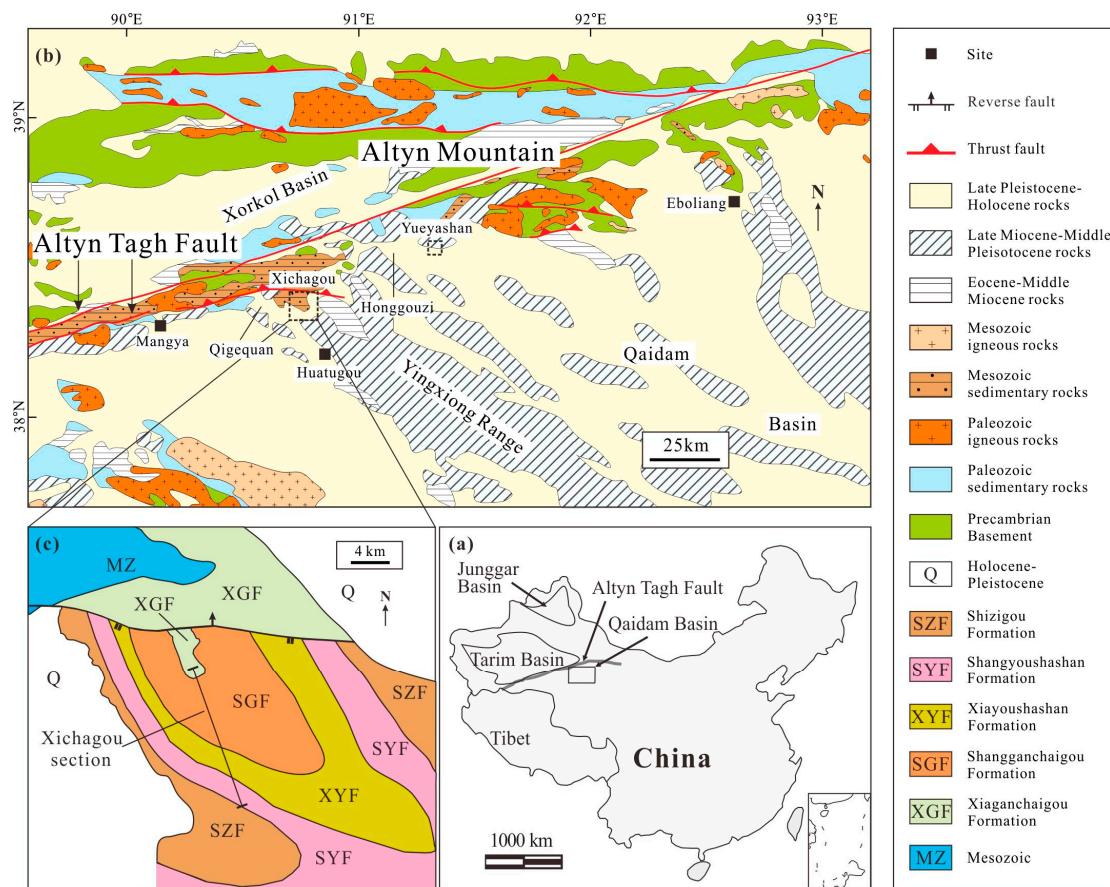


Figure 1. (a) Location of the Qaidam Basin and the Altyn Tagh Fault on the map of China; (b) The geological map of the central segment of the Altyn Tagh Fault and the western Qaidam Basin. The dashed rectangle marks the location of the Xichagou and Yueyashan sections; (c) The geological map of the Xichagou section (modified after [10]).

Some researchers accept the viewpoint that the cumulated offset along the ATF is 350–400 km and the strike-slip movement is always associated with tectonic uplift [1,5,8,11,13]. Liu et al. [14] reported that the collision between the India and Eurasia plates caused the initiation of strike-slip movement along the ATF in the deep crust during the 89–92 Ma period. Subsequently, this movement gradually extended from the deep to the surface during the middle Eocene. Yin et al. [11] suggested that crustal thickening in northern Tibet started earlier than 46 Ma, while the ATF has been active since approximately 49 Ma. Wang et al. [15] inferred from Cenozoic detrital zircon fission-track age in the northwestern Qaidam Basin that the Altyn Mountains did uplift and were exposed in the Paleocene–middle Eocene (65–50 Ma). Peter et al. [16] argued that the initial time of substantial slip on the ATF was in the Oligocene (ca. 30 Ma). Zhuang et al. [17] suggested the inception of substantial slip on the ATF in the early Oligocene was in response to accommodate the continuing indentation of India into Eurasia, and then the large-amplitude slip motion on the ATF occurred during the Oligocene–early Miocene. Furthermore, $^{40}\text{Ar}/^{39}\text{Ar}$ and fission track thermochronological results from the Altyn Mountains along the edges of the Qaidam Basin constrain rapid uplifting during the middle Oligocene–Miocene, which is attributed to significant strike-slip motion along the ATF during this period [12]. Meanwhile, a two-stage evolutionary model for the Altyn Tagh Fault, with the first stage of tectonic movement along the ATF starting in the Oligocene and the second stage occurring at ca. 13–16 Ma, was proposed by [7,10]. Differences exist in the tectonic characteristics of these two stages, as proposed in the research mentioned above. Ritts et al. [18] constrained the age of surface uplift and exhumation of the Altyn Mountains and the initiation of strike-slip motion on the ATF was 15 to 16 Ma. Lu et al. [19] held the

view that the fast strike-slip motion of the left-lateral ATF started between 22 and 15 Ma and was terminated between 15 and <6.3 Ma. Song et al. [20] suggested that the strike-slip activity of ATF occurred at 20.4 Ma, which is close to the ~24 Ma proposed by [9]. Additionally, the ages of the associated quartz vein and gypsum from the ATF were measured by electron spin resonance dating, which indicates that the tectonic activity of the ATF began in the middle Miocene [(12.5 ± 1.5 Ma)–(15.1 ± 1.5 Ma)] [21]. As shown by antecedent research on the ATF system, the crux of the debate lies in determining the epoch during which the left-lateral slip initiation occurred. Potential candidates for this epoch include the Paleocene, Eocene, Oligocene, or Miocene.

According to the analysis of previous data, it is apparent that the selection of research methods and sampling locations has a notable impact on the analysis of tectonic evolution in the ATF system. Currently, studies have demonstrated that sedimentary provenance analysis is a valuable tool for reconstructing past tectonic settings and comprehending the tectonic evolution history of large-scale source regions [22,23]. The Qaidam Basin, which contains a thick succession of Tertiary sediments, may provide significant information on tectonic activity and denudation processes in surrounding orogenic belts [24,25]. Thus, the sediments of the northwestern Qaidam Basin offer a new perspective on figuring out the evolution of the ATF and Altyn Mountains.

Heavy mineral assemblages in sandstones and the geochemical composition of heavy minerals are widely used in sedimentary provenance analysis [26]. The characteristics of heavy minerals are closely related to the properties of the source rocks, and they can effectively reflect the characteristics of the source rock [23,27]. However, numerous studies indicate that the original provenance signal may be overprinted by complex processes, especially burial diagenesis and hydraulic sorting [26,27]. The hydraulic processes influence the relative abundance of minerals with different hydraulic behavior, which is controlled by grain size, density, and shape [27,28]. Some case studies show that unstable minerals undergo dissolution with increasing burial depth [29]. In order to overcome this obstacle, many methods have been proposed [26,28,30,31]. Despite this, heavy mineral data still offer insights into the mineralogical nature of the source terrains [27]. The geochemical data of heavy minerals can identify source rock types by accurate mineral composition and is less affected by transport, deposition, and diagenesis [26,32–34].

This study seeks to present an integrated provenance analysis of sediments from two critical sections adjacent to the ATF in the northwestern Qaidam Basin. Based on the comprehensive consideration of multiple methods, including mineral geochemistry, sandstone petrography, and heavy mineral analysis, temporal variations in the source areas of Tertiary sediments will be revealed. The obtained results contribute to reconstructing the tectonic history of the ATF system and establishing the relationship between sedimentary records and tectonic activities.

2. Geological Setting and Stratigraphy

2.1. Geologic Setting

The large-scale ATF and Altyn Mountains, located in the northwest of the Tibet Plateau, are important strike-slip fault zones and mountain systems, respectively, in Central Asia, which separate the Qaidam Basin from the Tarim Basin (Figure 1a). The Altyn Mountains exhibit lithological variations between their eastern and western parts. The rocks exposed in the western Altyn Mountains consist of medium- to high-grade metamorphic rocks, ophiolite, granite, Jurassic clastic rocks, and Ordovician flysch, while the eastern Altyn Mountains are comprised of Paleozoic and Mesozoic granites, diorite, and metamorphic rocks of the Proterozoic Dakendaban Group [35–39].

The northwestern Qaidam Basin, which covers an area of approximately 1.5×10^4 km², is divided into several tectonic units such as Ganchaigou, Yueyashan, Honggouzi, and Qigequan. Two sections called the Xichagou outcrop section (XCG) and the Yueyashan well section (YYS) were selected for this study (Figure 1b), which are located in Ganchaigou and Yueyashan, respectively, near the southern limb of the ATF. Previous research has shown

that sediments in the Xichagou and the Yueyashan sections predominantly originate from the Altyn Mountains [10,40] (See Section 5.2 for more details), and their sedimentation may provide insights into the development of mountains and large-scale intracontinental faults.

2.2. Stratigraphy

The Paleogene and Neogene sediments in the northwestern basin have an average thickness of 4000 m and are composed of several formations. Based on magnetostratigraphy, paleontology, geochronology, and petrology [25,41–43], these formations, in ascending order, include Lulehe Formation (LHF: >44 Ma), Xiaganchaigou Formation (XGF: ~44 to ~35.5 Ma), Shangganchaigou Formation (SGF: ~35.5 to ~22 Ma), Xiayouhashan Formation (XYF: ~22 to ~15.3 Ma), Shangyoushashan Formation (SYF: ~15.3 to ~8.1 Ma), and Shizigou Formation (SZG: ~8.1 to ~2.5 Ma) (Figures 1c and 2).

The LHF unconformably overlies the Cretaceous strata and is dominated by coarse red clastic rocks, representing alluvial fans and fluvial environments at the time [44,45]. The XGF is composed of conglomerate and sandstone, showing the grain size decreasing upward of the stratigraphy, and is interpreted as fluvial deposits. The SGF is mainly constituted of mudstone, limestone, siltstone, and fine sandstone with high maturity, which is believed to represent widespread lacustrine facies. Notably, large-scale turbidity current deposits occur in the middle SGF strata of the Xichagou section. Sediments in the XYF are predominantly comprised of siltstone and sandstone interbedded. The deposition environment of the XYF is interpreted as a delta or a shallow lake. Likewise, the SYF has lithological similarities with the XYF but with relatively larger debris particles, indicating a braided river setting during deposition. The SZG is constituted by massive conglomerates.

The Tertiary strata in the Xichagou and the Yueyashan sections, which we investigated, are well exposed. These sections serve as important survey areas with potential for investigating the tectonic evolution history of the ATF.

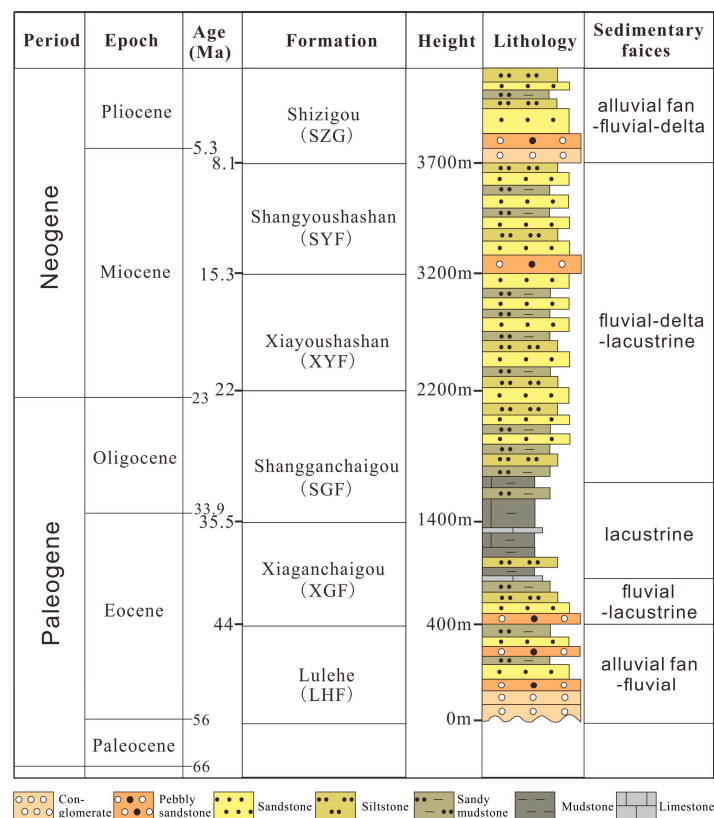


Figure 2. Comprehensive strata column of the Paleogene–Neogene in the Qaidam Basin (including the lithologic stratigraphy, facies, and geochronology). The geochronologic data is the synthetic analysis from [25,40,42,46–49].

3. Materials and Methods

A growing number of studies show that multiple methods could provide comprehensive and reliable interpretations of provenance, which can serve as a foundation for inferring regional tectonic history. In total, 32 samples were collected from both outcrop and well-core, primarily consisting of fluvial and deltaic sediments (Figure 3). We focused on sandstone deposits (from approximately 44 Ma to 8.1 Ma) and applied integrated data on sandstone composition and grain size, heavy minerals, mineral geochemistry, and lithofacies. Sample sites and corresponding strata are listed in Table 1.

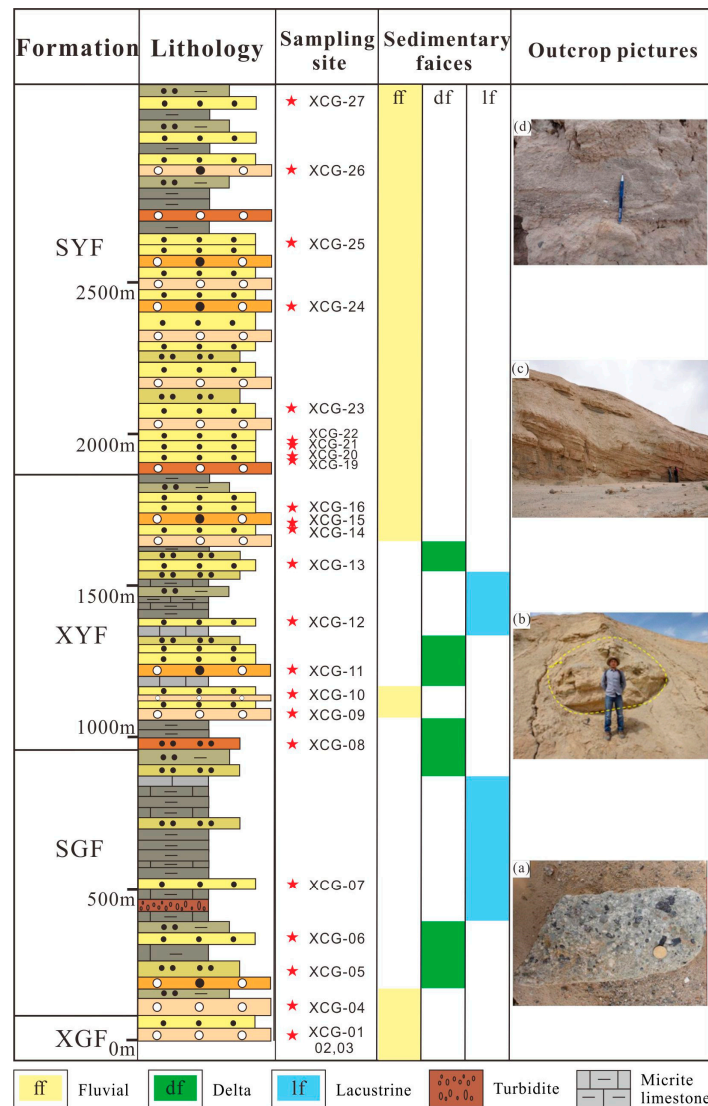
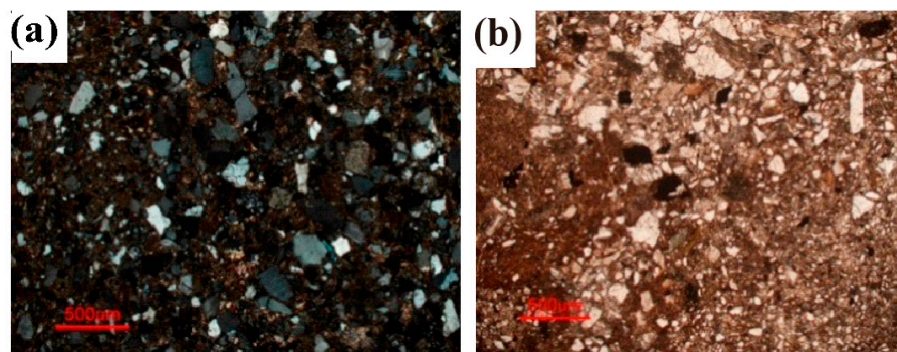


Figure 3. The lithology, facies, and outcrop pictures in the Xichagou section. The red stars mark the position of samples with labels from XCG-01 to XCG-27. (a) Fluvial conglomerates in the XGF; (b) The lenticular channel sand body in the XGF; (c) Lacustrine mudstone-marl interbeds in the SGF; (d) The graded bedding in the SYF.

Sandstone framework petrography is a useful method for provenance determination. The point-counting method [50,51] was used to calculate the major components of the sandstone, including single-crystal quartz, polycrystalline quartz, potassium feldspar, plagioclase, igneous rock debris, metamorphic rock debris, sedimentary rock debris, mica, and interstitial material. To ensure that the results were representative, at least 300 grains were counted for each sample. The grain size, sorting and roundness, mineral composition, texture, and diagenesis were studied using a polarizing microscope (Figure 4).

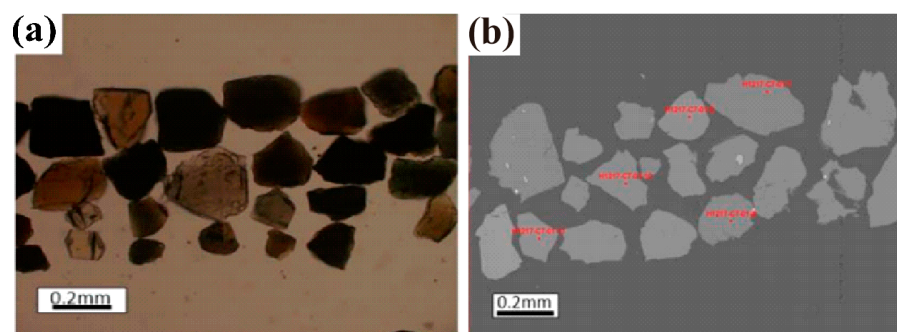
Table 1. Sample sites and corresponding strata.

Locality	Section	Formation				Analysis Items and Number of Samples		
		XGF	SGF	XYF	SYF	Composition Point Counting	Heavy Mineral Analysis	Mineral Geochemistry
Ganchaigou	XCG outcrop section	XCG-01~XCG-03	XCG-04~XCG-07	XCG-08~XCG-16	XCG-19~XCG-27	16	21	4
Yueyashan	YYS well section	YYS-01, YYS-02	YYS-03, YYS-04	YYS-05, YYS-06	YYS-07	0	6	4

**Figure 4.** (a) Sandstones of the XGF in the Xichagou section (crossed-polarized light); (b) Medium-grained sandstones of the XYF in the Xichagou section (plane-polarized light).

The heavy mineral analysis was performed on unweathered, medium- to coarse-grained sandstone samples [52]. The samples underwent the processes of crushing, oil removal, acidification, elutriation, drying, heavy mineral separation, and extraction. High-density liquid (tribromethane) was used for heavy mineral separation, with a density of 2.89 g/cm³ at 20 °C. Finally, at least 500 heavy minerals per sample were counted using the point-counting method [53] under a polarizing microscope. The grain size of heavy minerals used for analyses ranges from 0.2 to 0.4 mm.

Single-grain techniques serve as a basis for directly comparing them with the mineralogy of source rocks [26,27,34,54]. Geochemical composition analysis was done on detrital tourmalines and garnets from nine sandstone samples. The electron microprobe analyzer was used to randomly analyze 35–40 detrital grains of these minerals per sample (Figures 5 and 6). Detrital tourmalines were analyzed by the JXA 8230 electron microprobe, installed in the Chinese Academy of Geological Sciences of Beijing, China. The geochemical composition of the detrital garnets was acquired using a JXA 8100 electron microprobe at Peking University, Beijing, China (Figure 6).

**Figure 5.** Photomicrographs of typical detrital tourmalines in the northwestern Qaidam Basin. (a) Tourmalines in transmitted light; (b) Tourmalines in reflected light.

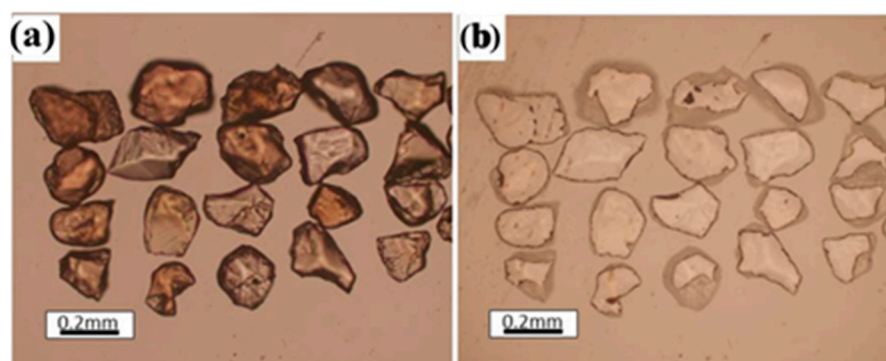


Figure 6. Photomicrographs of typical detrital garnets in the northwestern Qaidam Basin. (a) Garnets in transmitted light; (b) Garnets in reflected light.

4. Results

4.1. Sedimental Facies and Sandstone Petrography

Given that the Xichagou section represents a typical profile and contains the complete sequence of Paleogene-Neogene strata, spanning a total thickness of 3000 m, petrography, and petrology will be described below, using this section as an exemplar.

Three distinct sedimentary facies can be recognized in the study area (e.g., fluvial facies, delta facies, and lacustrine facies) (Figure 3). The main characteristics of sedimentary facies are described as follows:

The fluvial facies are predominantly composed of conglomerate, sandstone, and mudstone, with poor sorting and roundness of the particles in the sediments. Mudstone is the primary rock type of flood plain deposits, and conglomerate is deposited in the riverbed. Conglomerate exhibits imbricated arrangements and erosion structures at the bottom. Sedimentary structures such as tabular cross-bedding, trough cross-bedding, graded bedding, and the lenticular sand body are observed in the fluvial facies deposits. In the study area, braided river facies are characterized by channel bar deposits and various types of cross-bedding.

Delta facies are typically divided into delta plain, delta front, and prodelta subfacies. Delta facies mainly consist of medium-fine sandstone, siltstone, and mudstone. The delta plain subfacies include channels and interdistributary bays, characterized mainly by conglomerate and siltstone, respectively. Delta facies exhibit various sedimentary structures, including ripple bedding, horizontal bedding, lenticular bedding, and cross-bedding.

Lacustrine facies can be classified into lakeshore, shallow lake, semi-deep lake, and deep lake subfacies. The sediments of the lakeshore and the shallow lake mainly include mudstone and siltstone. Ripple bedding, lenticular bedding, and biogenic structures are usually exhibited in the facies. The deep-lake and semi-deep-lake facies are characterized by gray-black mudstone and marl, displaying horizontal bedding.

As previously mentioned, sediments at the top of the XGF comprise fluvial conglomerates and coarse-grained sandstones, while the SGF mainly consists of massive lacustrine mudstones, limestones, siltstones, and fine sandstones. Ripple marks, current bedding, and horizontal bedding are common sedimentary structures in SGF, and turbidity currents are also observed in the middle SGF. The sedimentary facies of SGF are interpreted as lacustrine facies occasionally interlaced with delta facies. The grain size roughly increases from the SGF to the SYF based on microscope observations, and sandstones start to replace lacustrine mudstones from the lower XYF. The XYF and SYF are dominated by conglomerates and pebbly sandstones, with an increase in the proportion of conglomerate clasts in the SYF. These two formations are interpreted to have been deposited in a fluvial environment (Figure 3). Except for that, most detrital grains in samples from the Xichagou section are angular to subangular and moderately sorted (Figure 4). The composition point-count method was used to obtain statistics, showing that the average Q:F:L ratios from the XGF

to the SYF in the Xichagou section are 63:21:16, 53:31:16, 51:43:7, and 48:41:12, while the average Qm:F:Lt ratios are 57:21:22, 47:31:22, 49:43:9, and 44:41:15 (Table S1 and Figure 7a).

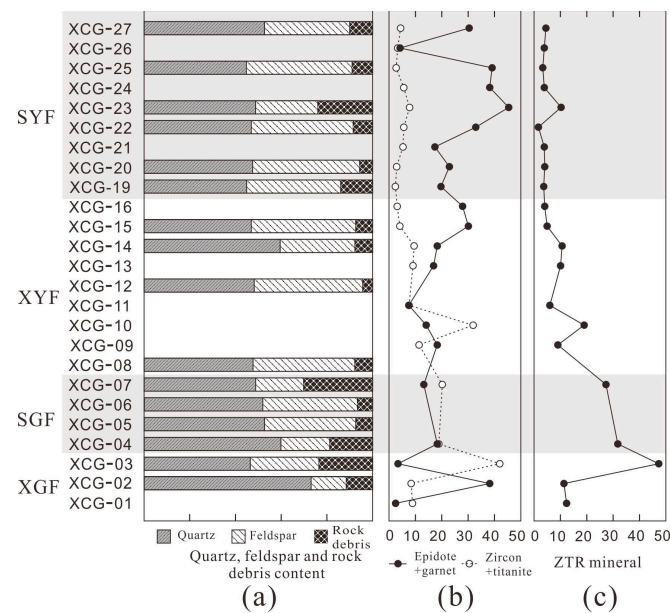


Figure 7. (a) Content of quartz, feldspar, and rock debris from the XGF to the SYF in the Xichagou section; (b) Contents of garnet and epidote, zircon and titanite from the XGF to the SYF in the Xichagou section. Black solid circles and hollow circles represent garnet and epidote, zircon and titanite severally; (c) Content of ZTR mineral from the XGF to the SYF in the Xichagou section.

4.2. Heavy Mineral Data

Here, 17 species of heavy minerals with varying abundances were identified in samples from the Xichagou and the Yueyashan sections, as listed in Table S2. The heavy mineral assemblages are dominated by hematite (average abundance, 39.2%; maximum abundance, 78.8%) and garnet (average abundance, 13.7%; maximum abundance, 37.9%). Subordinate minerals include zircon, leucoxene, anatase, titanite, magnetite, ilmenite, apatite, epidote, tourmaline, rutile, chlorite, pyroxene, and amphibole, with average abundances of 6.7%, 6.3%, 1.5%, 2.2%, 2.7%, 8.4%, 1.3%, 7.3%, 1.4%, 1.1%, 3.3%, 1.9%, and 2.7%, respectively. Monazite and biotite are minor constituents (average abundances, <1%).

According to the source characteristics and stability of the heavy minerals, eight heavy minerals were selected in this study to provide valuable information about provenance and source rocks. Typically, garnet, epidote, rutile, and chloritoid are mainly from metamorphic rocks, while zircon, titanite, apatite, and pyroxene are common in igneous rocks. In the Xichagou section, the content of garnet plus epidote from 21 effective samples ranges from 2.5 to 45.4, averaging 21.9, while the content of zircon plus titanite ranges from 2.4 to 42.1, averaging 10.2 (Table S2 and Figure 7b). The content of garnet plus epidote in six samples from the Yueyashan section ranges from 0 to 31.9, with an average of 17.8, while the content of zircon plus titanite ranges from 0.4 to 14.8, with an average of 4.1 (Table S2 and Figure 8b). Overall, both sections show that the content of garnet plus epidote is relatively higher than the content of zircon plus titanite in the upper formations.

When minimally influenced by sedimentary cycling factors (e.g., hydraulic sorting and burial diagenesis) [26–28,31,55], ZTR minerals, including zircon, tourmaline, and rutile, exhibit excellent stability, making their content a reliable indicator of the compositional maturity of sandstone samples based on a macro-level perspective [33,56]. The proportions of ZTR minerals reach their peak values at the top of XGF (47.2%) and the bottom of SGF (31.7%) in the Xichagou outcrop section (Table S2 and Figure 7c). Moreover, the maximum abundance of ZTR minerals in the Yueyashan section occurs in the XGF (5.4% and 4.6%),

with average abundances of 1.5%, 0.4%, and 2.6% in the SGF, XYF, and SYF, respectively (Table S2 and Figure 8c).

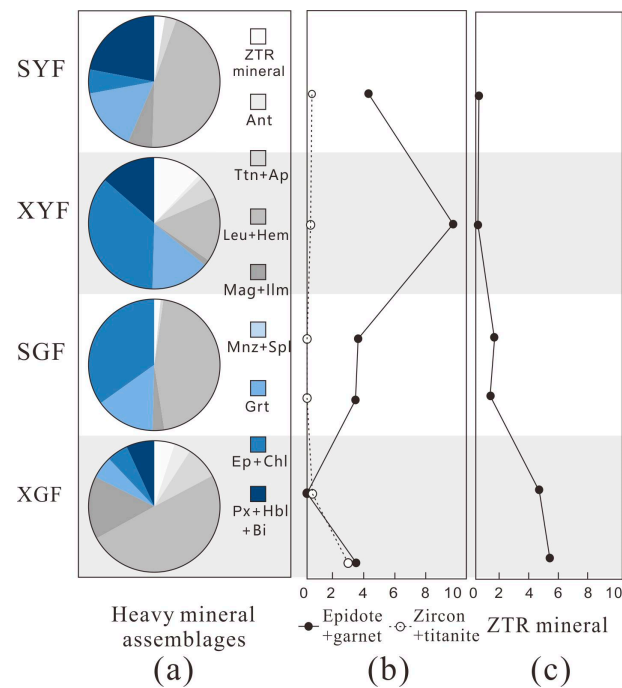


Figure 8. (a) Pie chart about heavy mineral assemblages from the XGF to the SYF in the Yueyashan section; (b) Contents of garnet and epidote, zircon and titanite from the XGF to the SYF in the Yueyashan section. Black solid circles and hollow circles represent garnet and epidote, zircon and titanite, respectively; (c) Content of ZTR mineral from the XGF to the SYF in the Yueyashan section.

4.3. Mineral Chemistry Data

Tourmaline is a complex borosilicate mineral with the general formula $(\text{Na, K, Ca}) (\text{Al, Fe, Li, Mg, Mn})_3 (\text{Al, Cr, Fe, V})_6 (\text{BO}_3)_3 (\text{Si}_6\text{O}_{18}) (\text{OH, F})_4$. Henry and Guidotti [57] suggested an $\text{Al}-\text{Al}_{50}\text{Fe}(\text{tot})_{50}-\text{Al}_{50}\text{Mg}_{50}$ ternary diagram with several fields based on the significant number of tourmaline geochemistry data, which helps to identify rock types. Garnet is usually classified as the calcium series $[\text{Ca}_3(\text{Al, Cr, Ti, Fe}^{3+})_2\text{Si}_3\text{O}_{12}]$ and aluminum series $[(\text{Mg, Fe}^{2+}, \text{Mn})_3\text{Al}_2\text{Si}_3\text{O}_{12}]$ [58]. A ternary $\text{Mg}-(\text{Fe}^{2+}+\text{Mn})-\text{Ca}$ diagram was proposed by using the garnet data for source rock discrimination [32]. Then the diagram was further improved by Mange et al. [59]. Geochemical data of tourmalines and garnets from eight samples in the Xichagou and Yueyashan sections are displayed on the aforementioned provenance-discriminant ternary diagrams (Figures 9 and 10). A more detailed analysis is stated as follows.

The percentage of tourmaline and garnet grains in the diagrams from the Xichagou section varies (Table 2 and Figure 9). Specifically, the percentage of tourmaline grains from the XGF and the SGF in fields B and C is higher than or equal to that in fields D, E, and F. However, the percentage of tourmaline grains in fields B and C of the ternary diagram decreases from the XYF to the SYF, while the percentage in fields D, E, and F increases significantly. For detrital garnet data of the XGF and SGF, it is mainly plotted in fields B and C. Notably, there is a sudden change above the XYF, with type C garnets almost disappearing and type A and B garnets rapidly increasing.

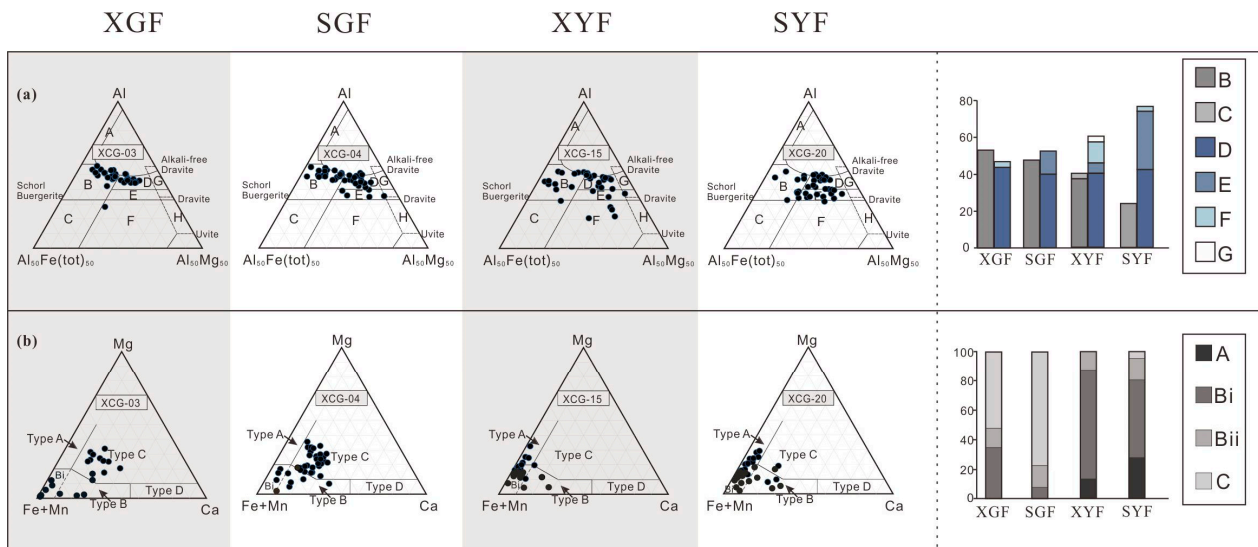


Figure 9. (a) The percentage of detrital tourmalines in the ternary diagrams from the Xichagou section. Field A: Li-rich granitoid pegmatites and aplites, Field B: Li-poor granitoids and their associated pegmatites and aplites, Field C: Fe³⁺-rich quartz-tourmaline rocks (hydrothermally altered granites), Field D: Meta-pelites and meta-psammities coexisting with an Al-saturating phase, Field E: Meta-pelites and meta-psammities not coexisting with an Al-saturating phase, Field F: Fe³⁺-rich quartz-tourmaline rocks, calc-silicate rocks, and meta-pelites, Field G: Low-Ca meta-ultramafics and Cr, V-rich meta-sediments, Field H: Meta-carbonates and meta-pyroxenites; (b) The percentage of detrital garnet grains in the ternary diagrams from the Xichagou section. Field A: High-grade granulite facies metamorphic sedimentary rock or charnockite and intermediate-felsic igneous rock from the deep crust, Field Bi: Intermediate-felsic magmatic rock, Field Bii: Intermediate-low-grade metasedimentary rock, Field C: High-grade metabasite, Field D: Metasomatic rocks or ultrahigh temperature metamorphosed calc-silicate granulites.

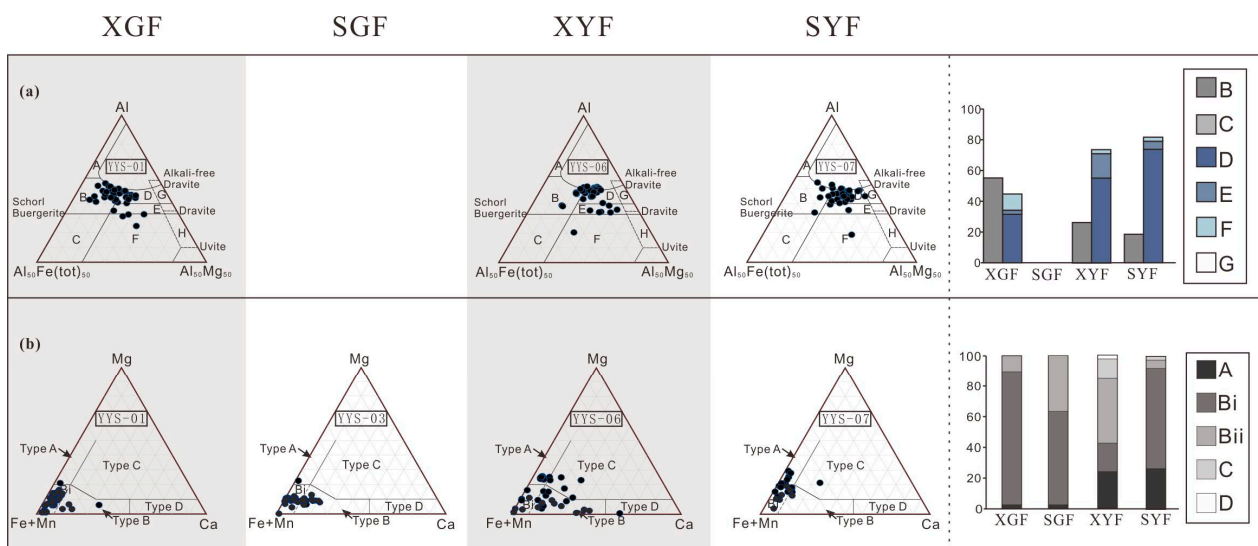


Figure 10. The percentage of detrital tourmalines (a) and garnets (b) in the ternary diagrams from the Yueyashan section.

Table 2. Geochemical data of tourmalines and garnets from the Xichagou section.

	Sample	Formation	Total	A	B	C	D	E	F	G
Tourma- lines	XCG-20	SYF	100.0	0.0	23.7	0.0	42.1	31.6	2.6	0.0
	XCG-15	XYF	100.0	0.0	37.1	2.9	40.0	5.7	11.4	2.9
	XCG-04	SGF	100.0	0.0	47.5	0.0	40.0	12.5	0.0	0.0
	XCG-03	XGF	100.0	0.0	56.3	0.0	40.6	0.0	3.1	0.0
	Sample	Formation	Total	A	Bi	Bii	C	D		
Garnets	XCG-20	SYF	100.0	27.5	52.5	15.0	5.0	0.0		
	XCG-15	XYF	100.0	13.2	73.7	13.1	0.0	0.0		
	XCG-04	SGF	100.0	0.0	7.5	15.0	77.5	0.0		
	XCG-03	XGF	100.0	0.0	34.8	13.0	52.2	0.0		

Figure 10 and Table 3 depict the percentages of tourmaline and garnet grains obtained from the Yueyashan section. In fields B and C, the percentage of tourmaline grains from the XGF exceeds that in fields D, E, and F. However, a significant change in the percentage of tourmaline grains is observed in the XYF and the SYF. Specifically, the proportion of grains in fields B and C decreases substantially, while that in fields D, E, and F increases. Detrital garnet data show that there are almost no type A and type C garnets in both XGF and SGF, while in the XYF, the percentage of both types of garnet grains has a significant increase. In the SYF, garnet grains are mainly concentrated in fields A and B.

Table 3. Geochemical data of tourmalines and garnets from the Yueyashan section.

	Sample	Formation	Total	A	B	C	D	E	F	G
Tourma- lines	YYS-07	SYF	100.0	0.0	18.4	0.0	73.7	5.3	2.6	0.0
	YYS-06	XYF	100.0	0.0	26.3	0.0	55.3	15.8	2.6	0.0
	YYS-01	XGF	100.0	0.0	55.3	0.0	31.6	2.6	10.5	0.0
	Sample	Formation	Total	A	Bi	Bii	C	D		
Garnets	YYS-07	SYF	100	26	66	5	3	0		
	YYS-06	XYF	100	24	18	42	13	3		
	YYS-03	SGF	100	3	61	37	0	0		
	YYS-01	XGF	100	3	87	11	0	0		

5. Discussions

5.1. Methodological Evaluation

To conduct the provenance analysis, we use an integrated approach that combines detrital framework composition, mineral chemistry, and heavy mineral data. Due to the complexity of geological processes, each dataset cannot fully provide comprehensive and accurate results. Hence, the use of multiple methods is essential. The design can be explained as follows:

Detrital framework composition analysis can provide valuable information about the source area. Statistical analysis results show variations from the XGF to the SYF, with the lowest concentration of rock fragment contents and the highest concentration of feldspar contents appearing in the XYF (Figure 7).

Heavy minerals are widely used as proxies for analyzing sediment provenance [27,56]. The contents and assemblages of heavy minerals are inherited from the source rocks, enabling estimation of the characteristics of sedimentary source rocks based on their mineral assemblages [33]. However, the complex overprinting processes (e.g., hydraulic sorting and burial diagenesis) may affect heavy mineral distribution in sandstones [26–28,31,55]. For an accurate provenance interpretation, it is essential that the parameters used are inherited from the source area rather than extensively modified by processes operating during the sedimentary cycle. Among these processes, the most critical factors are hydraulics and diagenesis. In our study, the heavy minerals used for analysis have similar grain sizes

and densities and are predominantly equant in shape. Therefore, hydraulic sorting has minimal impact on the distribution of heavy minerals in this study [55]. As burial increases, the diversity of heavy minerals decreases steadily due to the dissolution of heavy mineral species. Some heavy minerals would be eliminated, starting with amphibole, followed by epidote, titanite, kyanite, staurolite, and garnet [27]. Compared to other heavy minerals, amphibole is more susceptible to dissolution due to burial diagenesis [27,29]. However, the amphibole/titanite ratio, amphibole/garnet ratio, and epidote/titanite ratio do not show a significant increasing trend from XGF to SYF. Similarly, there is no obvious decreasing trend in the garnet/titanite ratio (Figure 11). This means that the diagenetic burial had no obvious effect on heavy minerals in this study.

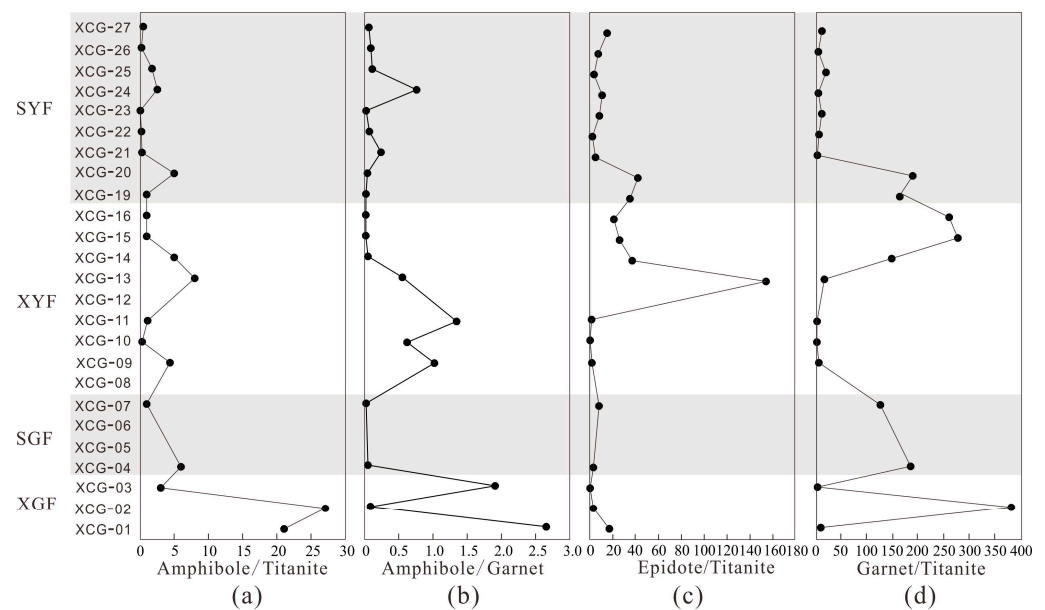


Figure 11. (a) The amphibole/titanite ratio from the XGF to the SYF in the Xichagou section; (b) The amphibole/garnet ratio from the XGF to the SYF in the Xichagou section; (c) The epidote/titanite ratio from the XGF to the SYF in the Xichagou section; (d) The garnet/titanite ratio from the XGF to the SYF in the Xichagou section.

Most important of all, the geochemical composition of heavy minerals could give direct information on the source rock. Unlike heavy mineral data, the strength of such studies lies in minimizing possible effects of intrastratal dissolution during diagenesis, as well as of sedimentary processes during transport of the detrital minerals [34,60]. Although differences in the sizes of garnet and tourmaline crystals within the source area could lead to distinctions in hydraulic sorting of garnet compositional types between coarse-grained and fine-grained sandstones, several studies indicate that this effect is generally minor [60]. The percentage of tourmaline and garnet grains in the ternary diagrams from the Xichagou section and the Yueyashan section shows a significant change in the XYF (Figures 9 and 10). The implementation of this method ensures that our results are convincing and reliable. Therefore, mineral chemical data is the main evidence to support the conclusion, while detrital framework composition and heavy mineral data provide extra supporting evidence.

5.2. Provenance of the Northwestern Qaidam Basin in the Tertiary

Provenance analysis has been proposed as one of the essential prerequisites for understanding the evolution of source areas and reconstructing the ancient landscape [34,61]. The tectonic activities of the Altyn Mountains and ATF are closely related. Before discussing the tectonic evolution of the ATF, the provenance of the Tertiary sediments in the northwestern Qaidam Basin needs to be further clarified. Based on $^{40}\text{Ar}/^{39}\text{Ar}$ dating of detrital white mica (350–450 Ma), Rieser et al. [62] presumed that the Altyn Mountains were the main

source of the sediments in the northwestern Qaidam Basin. In addition, according to samples from outcrops and well cores, the massive Tertiary alluvial conglomerates and large debris fans observed in Ganchaigou both indicate a nearby source [10]. In addition, for the Oligocene, Hanson [63] identified the direction of paleocurrents in the northwestern Qaidam Basin and found divergent paleocurrent directions with a mean vector directed toward the SE using the surface samples from Ganchaigou. Until now, it has been well accepted that the Altyn Mountains may contribute more sediment to the northwestern Qaidam Basin. Therefore, the sediments in the Xichagou and Yueyashan sections are primarily sourced from the Altyn Mountains.

Sandstone compositions result from a complex interplay between provenance and factors that operate during the sedimentation cycle [27]. Typical heavy mineral assemblages in sandstones are regularly regarded as important indications of provenances, which are capable of revealing source rock types [64,65]. For instance, zircon, titanite, and apatite normally exist in intermediate-felsic magmatic rocks, while pyroxene is mainly from ultramafic-intermediate magmatic rocks [64,65]. These minerals are often referred to as ZTAP minerals. In contrast, garnet, epidote, rutile, and chlorite (GERC minerals for short) are common minerals in multiple types of metamorphic rocks [66], which are considered to be source rock indicators for metamorphic rocks [53]. As is shown in the Xichagou and Yueyashan sections (Table S2), the proportions of ZTAP minerals (average: 13.19% in the Xichagou section; 10.40% in the Yueyashan section) and GERC minerals (average: 22.40% in the Xichagou section; 35.90% in the Yueyashan section) are fairly similar, respectively. Deposit zones with the same or similar heavy mineral assemblages are commonly affected by the same provenance area. Therefore, this similarity of ZTAP and GERC may imply the same provenance area for these sections in the northwestern Qaidam Basin. In addition, the heavy mineral assemblages are dominated by ZTAP and GERC minerals, unraveling felsic magmatic rocks and metamorphic rocks as source rocks.

The geochemical composition of heavy minerals can also identify source rock types by accurate mineral composition and effectively reduce the impact of transport, deposition, and diagenesis [27,34,60]. Two ideal heavy minerals, tourmaline, and garnet, are used to identify the provenance characteristics in this study. Tourmaline grains are predominantly plotted in fields B, D, and E on $\text{Al}-\text{Al}_{50}\text{Fe}(\text{tot})_{50}-\text{Al}_{50}\text{Mg}_{50}$ ternary diagrams. The result shows that the characteristics of source rock resemble Li-poor granitoids, meta-pelites, and meta-psammities (Figures 9 and 10). Additionally, garnet grains are mostly plotted in field B, suggesting that the source rock characteristics are similar to those of intermediate-felsic magmatic and intermediate-low-grade metasedimentary rock (Figures 9 and 10). These results are consistent with what we discussed above, indicating that the primary sources of deposition in the northwestern Qaidam Basin are dominated by intermediate-felsic magmatic rocks and metamorphic rocks.

The Altyn Mountains, located in the northwest of the Qaidam Basin, mainly consist of the Paleozoic to Mesozoic intermediate-felsic igneous rocks, the Neoproterozoic, Lower Paleozoic, and Paleoproterozoic metamorphic rocks [67–69]. Thus, the Paleozoic to Mesozoic igneous rocks, as well as the Neoproterozoic, Lower Paleozoic, and Paleoproterozoic metamorphic rocks from the Altyn Mountains may be the source rocks of the Yueyashan and the Xichagou sections (more details are listed in Table S3).

Consequently, in combination with previous studies, heavy mineral assemblages, and the geochemical composition of detrital minerals, it can be concluded that the Tertiary sediments of the Xichagou section and the Yueyashan section are mainly sourced from the Altyn Mountains (Figure 1 and Table S3).

5.3. Analysis of Depositional Records

5.3.1. Depositional Records in the Xichagou Outcrop Section

Sedimentary characteristics in the Xichagou outcrop section are critical to reflecting the denudation process of the Altyn Mountains. The depositional records in the Xichagou section exhibit varying source rock types. The percentage of tourmaline grains in fields

B and C, representing magmatic rocks, shows a decreasing trend, particularly from the SGF to the SYF. It is inferred that the total contribution of metamorphic rocks increases upsection (especially metasedimentary rocks of all metamorphic grades), although the contribution of high-grade metabasites declines markedly (as evidenced by the decrease in type C garnets), which means types of detrital garnets of the XYF also show an obvious change (Figure 9). Moreover, a dramatic decrease in felsic components observed at the XYF is also indicated by an increase in garnet and epidote content and a decrease in zircon and titanite content (Figure 7b).

The content of quartz displays a decreasing trend. The lowest concentration of the rock fragment contents appears in the XYF (Figure 7a). Simultaneously, the proportions of ZTR minerals decrease rapidly from the top of the SGF upwards to the SYF and reduce markedly at the bottom of the XYF (Figure 7c). These features suggest that the stability of the sandstones roughly decreases through time (Figure 7), particularly during the transition from the XYF to the SYF. Furthermore, the sandstones in the late Eocene–late Oligocene are relatively stable from the top of the XGF to the SGF, which is also consistent with the characteristics reflected by sedimental facies. Although large-scale turbidity current deposits occur in the middle SGF, it may imply that tectonic activities existed in the local area of the Altyn Mountains.

Therefore, the evidence demonstrated that the Altyn Mountains were relatively calm during the late Eocene–Oligocene, followed by increased activity after the early Miocene. Additionally, it can be inferred that the uplift event of the Altyn Mountains results in changes in the composition of source rocks and the stability of sediments.

5.3.2. Depositional Records in the Yueyashan Section

The sedimentary characteristics observed in the Yueyashan section provide additional insight into the evolutionary history of the Altyn Mountains. The source rock types for the sandstones in the Yueyashan section also undergo significant changes. The amount of tourmalines derived from intermediate-felsic magmatic rocks in the XGF is slightly more than that supplied by metasedimentary rocks. Conversely, tourmaline grains in other strata mainly come from metasedimentary rocks (fields D, E, and F). Fewer tourmaline grains are from intermediate-felsic magmatic rocks in the XYF, with a content of around 25% (Figure 10). The proportion of garnet and epidote from metamorphic rocks in the Yueyashan section has increased obviously since the SGF (Figure 8). In addition, the same features can be observed in the geochemical composition of garnets. In the XGF and SGF, detrital garnets principally belong to type B, suggesting that the rocks from the source area consist of intermediate-felsic magmatic rocks and intermediate-low metasedimentary rocks (Figure 10). All types of garnets are clearly present in the XYF, indicating that the types of metamorphic rocks are abundant in the source rocks (Figure 10). Moreover, the characteristics of detrital garnets differ in the SYF from the underlying strata. To be specific, the content of garnets from intermediate-low-grade metasedimentary rocks and high-grade metabasites is relatively reduced. In addition, the proportions of ZTR minerals show a noticeable decrease from the SGF to the XYF. Additionally, the content of unstable minerals such as pyroxene, amphibole, and biotite has become relatively enriched from the SGF to the XYF (Figure 8). Therefore, from the late Oligocene to the early Miocene, it can be speculated that the high-grade metamorphic rocks were heavily denuded and moved into the basin, leading to obvious changes in the components of the source rocks. Furthermore, tectonic activities in the Altyn Mountains were much more likely initiated at this time, exactly as indicated by the information analyzed in the Xichagou section.

5.4. Tectonic Evolution of the Altyn Tagh Fault

The Altyn Mountains mainly affect the geography of our study area, while the ATF has exerted a significant influence on the tectonic activity of the Altyn Mountains. Therefore, the Cenozoic uplift of the Altyn Mountains is commonly attributed to the strike-slip movement

along the ATF according to apatite fission-track dating and Ar-Ar dating [13,70–72]. This viewpoint is also adopted in this paper.

Sedimentary facies studies in Figure 12 show that, compared with the Miocene deposits, the lakeshore in the northwestern Qaidam Basin of the late Eocene–Oligocene is relatively closer to the ATF, and the center of the lake basin is closer to the ATF as well. Characteristics of the Xichagou section show that the largest lake flooding surface appears in the lower part of the SGF, suggesting that the sedimentary environment of the northwestern Qaidam Basin is stable, while the transformation interface of sedimentary facies is roughly at the bottom of the XYF. Videlicet, progradational sandstones started to replace widespread lacustrine mudstones in the early Miocene (Figure 2). According to petrographic analysis, the northwestern Qaidam Basin was tectonically relatively quiescent from the late Eocene through the Oligocene (though gravity flow deposited occasionally), which corresponds with the tectonic setting of the ATF system was relatively calm at that time. Then, active tectonics began on the ATF after the Oligocene.

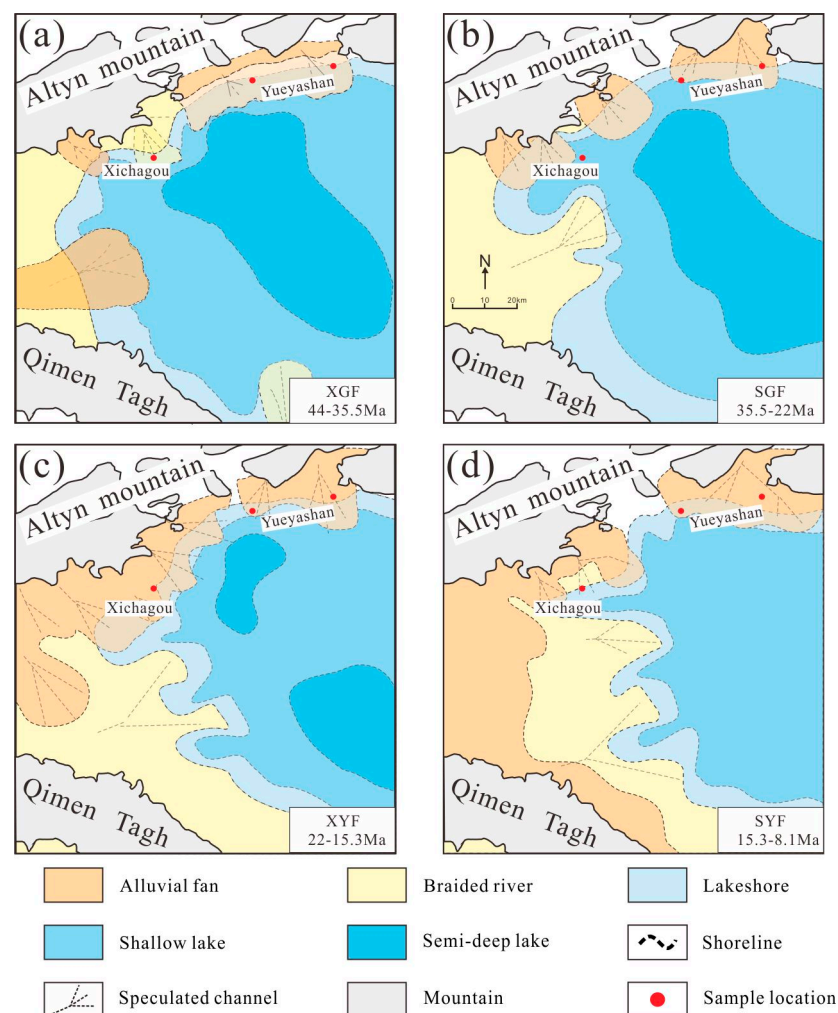


Figure 12. Diagrams of deposition facies from the XGF to the SYF in the northwestern Qaidam Basin. (a) XGF (E3); (b) SGF (N1); (c) XYF (N21); (d) SYF (N22) (modified after [73]).

Our results from two sections in the Qaidam Basin reveal that the parent rocks of the Altyn Mountains also changed significantly during the early Miocene, with a decrease in sediment maturity. At this time, the proportion of magmatic rocks decreased, the high-grade metabasites changed abruptly, and the high-grade metasedimentary rocks were largely denuded. These features imply that exhumation and denudation rates of metasedimentary rocks of various grades increased in the Altyn Mountains. The distinct change in

provenance characteristics reflects the Altyn Mountains' uplift activities. The activities of the ATF are closely intertwined with the genesis of the Altyn Mountains [1,2,70–72]. We thus suppose that the ATF began to undergo large-scale tectonic activity at about 22 Ma (the early–middle Miocene). An angular discordance between the SGF and the XYF is also found in the seismic section of the southern Altyn Mountains front zones [2], which still supports the view that activities of the ATF began in the early Miocene. Previous studies [9,74,75] considered that the tectonic activity of the ATF was mainly a strike-slip movement. After the Miocene, the stability of sandstones in the Xichagou and Yueyashan sections continued to decrease, indicating that the active tectonic setting of the ATF represented an ongoing trend.

6. Conclusions

Based on the geological background and previous studies, a detailed analysis of the petrology, heavy mineralogy, and single mineral geochemistry of the sediments in the northwestern Qaidam Basin (e.g., the Xichagou section and the Yueyashan well section) allows us to draw the following conclusions:

1. Sediments of the Xichagou and Yueyashan sections are mainly from the Altyn Mountains, which provide terrific geologic materials to study the tectonic evolution history of the ATF.
2. It is vital to determine the time limit of Tertiary tectonic activities in the ATF, which can limit the deformation time of the northern Tibet Plateau. We consider a two-stage evolution of the ATF during the Tertiary: (1) From the late Eocene to the Oligocene, there was no strong tectonic activity in the ATF; (2) In the early Miocene (~22 Ma), the ATF underwent large-scale tectonic activation. The significant changes were recorded by the petrology, heavy mineral characteristics, and stability of the sediments provided to the basin. It is likely to be a strike-slip tectonic activity of the ATF, accompanied by an uplift of the Altyn Mountains. Additionally, the active tectonic setting of the ATF was sustained after the Miocene.

Supplementary Materials: The following supporting information can be downloaded at: <https://www.mdpi.com/article/10.3390/min13081076/s1>, Table S1: Composition Point-count data in the Xichagou section; Table S2: Heavy mineral data in the Xichagou and the Yueyashan sections; Table S3: Provenance analysis index from the Xichagou and the Yueyashan sections.

Author Contributions: Validation, formal analysis, writing—original draft preparation, L.B.; conceptualization, methodology, formal analysis, L.F.; writing—review and editing, project administration, P.G.; resources, supervision, D.Z. All authors have read and agreed to the published version of the manuscript.

Funding: This research was funded by the National Key R&D Program of China, grant number 2021YFA0719000, and the National Nature Science Foundation of China, grant number 42141021.

Data Availability Statement: Not applicable.

Conflicts of Interest: The authors declare no conflict of interest.

References

1. Liu, Y.J.; Neubaue, F.; Genser, J.; Ge, X.H.; Takasu, A.; Yuan, S.H.; Chang, L.H.; Li, W.M. Geochronology of the initiation and displacement of the Altyn Strike-Slip Fault, western China. *J. Asian Earth Sci.* **2007**, *29*, 243–252. [[CrossRef](#)]
2. Liu, Y.J.; Neubaue, F.; Ge, X.H.; Genser, J.; Yuan, S.H.; Li, W.M.; Gong, Q.L.; Chen, Y.Z. Geochronology of the initiation and displacement of the Altyn Strike-Slip Fault and the uplift history of the Altyn Mountains. *Chin. J. Geol.* **2007**, *42*, 134–146.
3. Bendick, R.; Bilham, R.; Freymueller, J.; Lareon, K.; Yin, G. Geodetic evidence for a low slip rate in the Altyn Tagh fault system. *Nature* **2000**, *404*, 69–72. [[CrossRef](#)]
4. Tapponnier, P.; Ryerson, F.J.; Van der Woerd, J.; Mériaux, A.S.; Lasserre, C. Long-term slip rates and characteristic slip: Keys to active fault behavior and earthquake hazard: Comptes Rendus. *Académie Sci. Paris IIA* **2001**, *333*, 483–494. [[CrossRef](#)]
5. Yue, Y.; Ritts, B.D.; Graham, S.A.; Wooden, J.L.; Gehrels, G.E.; Zhang, Z. Slowing extrusion tectonics: Lowered estimate of post-Early Miocene slip rate for the Altyn Tagh fault. *Earth Planet. Sci. Lett.* **2003**, *217*, 111–122. [[CrossRef](#)]

6. Cowgill, E.; Yin, A.; Harrison, T.M.; Xiaofeng, W. Reconstruction of the Altyn Tagh fault based on U-Pb geochronology: Role of back thrusts, mantle sutures, and heterogeneous crustal strength in forming the Tibetan Plateau. *J. Geophys. Res. Solid Earth* **2003**, *108*, 1–7. [[CrossRef](#)]
7. Yue, Y.; Liu, J.G. Two-stage evolution model for the Altyn Tagh fault, China. *Geology* **1999**, *27*, 227–230. [[CrossRef](#)]
8. Ritts, B.D.; Biffi, U. Magnitude of post-Middle Jurassic (Bajocian) displacement on the central Altyn Tagh fault system, northwest China. *Geol. Soc. Am. Bull.* **2000**, *112*, 61–74. [[CrossRef](#)]
9. Chen, Y.; Gilder, S.; Halim, N.; Cogné, J.P.; Courtillot, V. New paleomagnetic constraints on central Asian kinematics: Displacement along the Altyn Tagh fault and rotation of the Qaidam Basin. *Tectonics* **2002**, *21*, 6–1–6–19. [[CrossRef](#)]
10. Wu, L.; Xiao, A.C.; Ang, S.F.; Wang, L.Q.; Mao, L.G.; Wang, L.; Dong, Y.P.; Xu, B. Two-stage evolution of the Altyn Tagh Fault during the Cenozoic: New insight from provenance analysis of a geological section in NW Qaidam Basin, NW China. *Terra Nova* **2012**, *24*, 387–395. [[CrossRef](#)]
11. Yin, A.; Rumelhart, P.E.; Cowgill, E.; Butler, R.; Harrison, T.M.; Ingersoll, R.V.; Cooper, K.; Zhang, Q.; Wang, X.F. Tectonic history of the Altyn Tagh fault in northern Tibet inferred from Cenozoic sedimentation. *Geol. Soc. Am. Bull.* **2002**, *114*, 1257–1295. [[CrossRef](#)]
12. Wang, Y.; Zhang, X.M.; Wang, E.; Zhang, J.F.; Li, Q.; Sun, G.H. $^{40}\text{Ar}/^{39}\text{Ar}$ thermochronological evidence for formation and Mesozoic evolution of the northern-central segment of the Altyn Tagh fault system in the northern Tibetan Plateau. *Geol. Soc. Am. Bull.* **2005**, *117*, 1336–1346. [[CrossRef](#)]
13. Yuan, S.H.; Liu, Y.J.; Ge, X.H.; Wu, G.D.; Hu, Y.Y.; Guo, X.Z.; Li, W.M. Uplift period of the northern margin of the Qinghai-Tibet Plateau: Evidences from the Altyn Mountains and Qaidam Basin. *Acta Petrologica Mineralogica* **2008**, *27*, 413–421.
14. Liu, Y.J.; Ge, X.H.; Ye, H.W.; Liu, J.L. Strike-Slip Model for Altyn Tagh Fault developed since Late Mesozoic. *Acta Geosci. Sin.* **2001**, *22*, 23–28.
15. Wang, Y.; Zheng, J.; Sun, G.; Zheng, Y.; Liu, X. Early Cenozoic Altyn Mountains Uplift Recorded by Detrital Zircon Fission Track Age in Northwest Qaidam Basin. *J. Jinlin Univ.* **2015**, *45*, 1447–1459.
16. Peter, R.; An, Y.; Robert, B.; Richards, D.; Wang, X. Oligocene initiation of deformation of northern Tibet, evidence from the Tarim basin, NW China. *Geol. Soc. Am. Abstr. Programs* **1997**, *29*, A143.
17. Zhuang, G.; Hourigan, J.K.; Ritts, B.D.; Kent-Corson, M.L. Cenozoic multiple-phase tectonic evolution of the northern Tibetan Plateau: Constraints from sedimentary records from Qaidam basin, Hexi Corridor, and Subei basin, northwest China. *Am. J. Sci.* **2011**, *311*, 116–152. [[CrossRef](#)]
18. Ritts, B.D.; Yue, Y.J.; Graham, S.A.; Sobel, E.R.; Abbink, O.A.; Stockli, D. From sea level to high elevation in 15 million years: Uplift history of the northern Tibetan Plateau margin in the Altyn Shan. *Am. J. Sci.* **2008**, *308*, 657–678. [[CrossRef](#)]
19. Lu, H.J.; Fu, B.H.; Shi, P.L.; Ma, Y.X.; Li, H.B. Constraints on the uplift mechanism of northern Tibet. *Earth Planet. Sci. Lett.* **2016**, *453*, 108–118. [[CrossRef](#)]
20. Song, X.; Cheng, X.; Lin, X.; Gao, S. Cenozoic uplifting history of the Altyn Mountains: Sedimentary records from the Ruoqiang Sag, southeastern Tarim Basin. *Chin. J. Geol.* **2019**, *54*, 330–344.
21. Li, M.M.; Tang, L.J.; Qiu, H.J.; Wang, P.H.; Zhen, S.J. Evidences from ESR dating for structural deformation of Altyn Tagh Fault System since Middle Miocene. *J. Earth Sci. Environ.* **2015**, *37*, 58–65.
22. Jian, X.; Guan, P.; Zhang, D.W.; Zhang, W.; Feng, F.; Liu, R.J.; Lin, S.D. Provenance of Tertiary sandstone in the northern Qaidam basin, northeastern Tibetan Plateau: Integration of framework petrography, heavy mineral analysis and mineral chemistry. *Sediment. Geol.* **2013**, *290*, 109–125. [[CrossRef](#)]
23. Von Eynatten, H.; Gaupp, R. Provenance of Cretaceous synorogenic sandstones in the Eastern Alps: Constraints from framework petrography, heavy mineral analysis and mineral chemistry. *Sediment. Geol.* **1999**, *124*, 81–111. [[CrossRef](#)]
24. Metivier, F.; Gaudemer, Y.; Tapponnier, P.; Meyer, B. Northeastward growth of the Tibet plateau deduced from balanced reconstruction of two depositional areas: The Qaidam and Hexi Corridor basins, China. *Tectonics* **1998**, *17*, 823–842. [[CrossRef](#)]
25. Sun, Z.; Yang, Z.; Pei, J.; Ge, X.; Wang, X.; Yang, T.; Li, W.; Yuan, S. Magnetostratigraphy of Paleogene sediments from northern Qaidam Basin, China: Implications for tectonic uplift and block rotation in northern Tibetan plateau. *Earth Planet. Sci. Lett.* **2005**, *237*, 635–646. [[CrossRef](#)]
26. Morton, A.C.; Hallsworth, C. Identifying provenance-specific features of detrital heavy mineral assemblages in sandstones. *Sediment. Geol.* **1994**, *90*, 241–256. [[CrossRef](#)]
27. Morton, A.C.; Hallsworth, C.R. Processes controlling the composition of heavy mineral assemblages in sandstones. *Sediment. Geol.* **1999**, *124*, 3–29. [[CrossRef](#)]
28. Razum, I.; Luar-Oberiter, B.; Zaccarini, F.; Babi, L.; Miko, S.; Hasan, O.; Ilijani, N.; Beqiraj, E.; Pawlowsky-Glahn, V. New sediment provenance approach based on orthonormal log ratio transformation of geochemical and heavy mineral data: Sources of eolian sands from the southeastern Adriatic archipelago. *Chem. Geol.* **2021**, *583*, 120451. [[CrossRef](#)]
29. Morton, A. Stability of Detrital Heavy Minerals in Tertiary Sandstones from the North Sea Basin. *Clay Miner.* **1984**, *19*, 287–308. [[CrossRef](#)]
30. Verhaegen, J.; Weltje, G.J.; Munsterman, D. Workflow for analysis of compositional data in sedimentary petrology: Provenance changes in sedimentary basins from spatio-temporal variation in heavy-mineral assemblages. *Geol. Mag.* **2018**, *156*, 1111–1130. [[CrossRef](#)]
31. Eynatten, H.V. Statistical modelling of compositional trends in sediments. *Sediment. Geol.* **2004**, *171*, 79–89. [[CrossRef](#)]

32. Morton, A.C.; Hallsworth, C.R.; Chalton, B. Garnet compositions in Scottish and Norwegian basement terrains: A framework for interpretation of North Sea sandstone provenance. *Mar. Pet. Geol.* **2004**, *21*, 393–410. [[CrossRef](#)]
33. Morton, A.; Whitham, A.; Fanning, C. Provenance of Late Cretaceous to Paleocene submarine fan sandstones in the Norwegian Sea: Integration of heavy mineral, mineral chemical and zircon age data. *Sediment. Geol.* **2005**, *182*, 3–28. [[CrossRef](#)]
34. Weltje, G.J.; Von Eynatten, H. Quantitative provenance analysis of sediments: Review and outlook. *Sediment. Geol.* **2004**, *171*, 1–11. [[CrossRef](#)]
35. Gehrels, G.E.; Yin, A.; Wang, X.F. Magmatic history of the northeastern Tibetan Plateau. *J. Geophys. Res.* **2003**, *108*, 1–5. [[CrossRef](#)]
36. Liu, L.; Chen, D.; Zhang, A.; Sun, Y.; Wang, Y.; Yang, J.; Luo, J. Ultrahigh pressure (>7 GPa) gneissic K-feldspar(-bearing) garnet clinopyroxenite in the Altyn Tagh, NW China: Evidence from clinopyroxene exsolution in garnet. *Sci. China Ser. D Earth Sci.* **2005**, *48*, 1000–1010. [[CrossRef](#)]
37. Rieser, A.B.; Neubauer, F.; Liu, Y.; Ge, X. Sandstone provenance of north-western sectors of the intracontinental Cenozoic Qaidam basin, western China: Tectonic vs. climatic control. *Sediment. Geol.* **2005**, *177*, 1–18. [[CrossRef](#)]
38. Yang, J.S.; Wu, C.L.; Zhang, J.X.; Shi, R.D.; Meng, F.C.; Wooden, J.; Yang, H.Y. Protolith of eclogites in the north Qaidam and Altyn UHP terrane NW China: Earlier oceanic crust? *J. Asian Earth Sci.* **2006**, *28*, 185–204. [[CrossRef](#)]
39. Mattinson, C.G.; Menold, C.A.; Zhang, J.X.; Bird, D.K. High-and ultrahigh pressure metamorphism in the North Qaidam and South Altyn Terranes, western China. *Int. Geol. Rev.* **2007**, *49*, 969–995. [[CrossRef](#)]
40. Wang, Y.D.; Zheng, J.J.; Zhang, W.L.; Li, S.Y.; Liu, X.W.; Yang, X.; Liu, Y.H. Cenozoic uplift of the Tibetan Plateau: Evidence from the tectonosedimentary evolution of the western Qaidam Basin. *Geoscience Front.* **2012**, *3*, 175–187. [[CrossRef](#)]
41. Yang, P.; Sun, Z.; Li, D.; Jing, M.; Xu, F.; Liu, H. Ostracoda extinction and explosion events of the Mesozoic–Cenozoic in Qaidam basin, northwest China. *J. Palaeogeogr.* **2000**, *2*, 69–74.
42. Fang, X.; Zhang, W.; Meng, Q.; Gao, J.; Wang, X.; King, J.; Song, C.; Dai, S.; Miao, Y. High-resolution magnetostratigraphy of the Neogene Huaitoutala section in the eastern Qaidam Basin on the NE Tibetan Plateau, Qinghai Province, China and its implication on tectonic uplift of the NE Tibetan Plateau. *Earth Planet. Sci. Lett.* **2007**, *258*, 293–306. [[CrossRef](#)]
43. Wang, X.; Qiu, Z.; Li, Q.; Wang, B.; Qiu, Z.; Downs, W.R.; Xie, G.; Xie, J.; Deng, T.; Takeuchi, G.T.; et al. Vertebrate paleontology, biostratigraphy, geochronology, and paleoenvironment of Qaidam Basin in northern Tibetan Plateau. *Palaeogeogr. Palaeoclimatol. Palaeoecol.* **2007**, *254*, 363–385. [[CrossRef](#)]
44. Fu, L.; Guan, P.; Jian, X.; Liu, R.J.; Feng, F.; An, Q.; Fan, C.F. Sedimentary genetic types of coarse fragment of Paleogene Lulehe Formation in the Qaidam basin and time limit of Tibetan Plateau Uplift. *Nat. Gas Geosci.* **2012**, *23*, 833–840.
45. Fu, L.; Guan, P.; Zhao, W.Y.; Wang, M.; Zhang, Y.; Lu, J.W. Heavy mineral feature and provenance analysis of Paleogene Lulehe Formation in the Qaidam basin. *Acta Petrol. Sin.* **2013**, *29*, 2867–2875.
46. Gao, J.P.; Li, S.X.; Dai, S.; Li, A.Y.; Peng, Y.H. Constraints of tectonic evolution in provenance from detrital zircon fission-track data of Cenozoic strata of Xichagou district in western Qaidam Basin. *J. Lanzhou Univ. (Nat. Sci.)* **2009**, *45*, 1–7.
47. Wang, Y.D.; Zhang, T.; Chi, Y.P.; Liu, Y.R.; Zhang, Z.G.; Li, S.Y.; Fang, X.M.; Zhang, Y.Z. Cenozoic uplift of the Tibetan Plateau: Evidence from tectonic-sedimentary evolution of the Western Qaidam Basin. *Earth Sci. Front.* **2011**, *18*, 141–150.
48. Lu, H.; Xiong, S. Magnetostratigraphy of the Dahonggou section, northern Qaidam Basin and its bearing on Cenozoic tectonic evolution of the Qilian Shan and Altyn Tagh Fault. *Earth Planet. Sci. Lett.* **2009**, *288*, 539–550. [[CrossRef](#)]
49. Meng, Q.Q. *Fine Magnetic Stratigraphy and Sediments from the Northern Qaidam Basin Response to Tectonic Activities in Late Cenozoic*; Lanzhou University: Lanzhou, China, 2008.
50. Ingersoll, R.V.; Bullard, T.F.; Ford, R.L.; Grimm, J.P.; Pickle, J.D.; Sares, S.W. The effect of grain size on detrital modes: A test of the Gazzi–Dickinson point-counting method. *J. Sediment. Petrol.* **1984**, *54*, 103–116.
51. Dickinson, W.R. Interpreting provenance relations from detrital modes of sandstones. *Proven. Arenites* **1985**, *148*, 333–336.
52. Hallsworth, C.R.; Chisholm, J.I. Provenance of late Carboniferous sandstones in the Pennine Basin (UK) from combined heavy mineral, garnet geochemistry and palaeocurrent studies. *Sediment. Geol.* **2008**, *203*, 196–212. [[CrossRef](#)]
53. Mange, M.A.; Maurer, H.F.W. *Heavy Minerals in Colour*, 1st ed.; Chapman and Hall: London, UK, 1992; pp. 1–145.
54. Sabeen, H.M.; Ramanujam, N.; Morton, A.C. The provenance of garnet: Constraints provided by studies of coastal sediments from southern India. *Sediment. Geol.* **2002**, *152*, 279–287. [[CrossRef](#)]
55. Weltje, G.J. A quantitative approach to capturing the compositional variability of modern sands. *Sediment. Geol.* **2004**, *171*, 59–77. [[CrossRef](#)]
56. Hubert, J.F. A zircon-tourmaline-rutile maturity index and the interdependence of the composition of heavy mineral assemblages with the gross composition and texture of sandstones. *J. Sediment. Res.* **1962**, *32*, 440–450.
57. Henry, D.J.; Guidotti, C.V. Tourmaline as a petrogenetic indicator mineral: An example from the staurolite-grade metapelites of NW Maine. *Am. Mineral.* **1985**, *70*, 1–15.
58. Deer, W.A.; Howie, R.A.; Zussman, J. *Rock-Forming Minerals*, 2nd ed.; Geological Society: London, UK, 1997; pp. 1–919.
59. Mange, M.A.; Morton, A.C. Chapter 13 Geochemistry of Heavy Minerals. *Dev. Sedimentol.* **2007**, *58*, 345–391.
60. Tsikouras, B.; Pe-Piper, G.; Piper, D.J.W.; Schaffer, M. Varietal heavy mineral analysis of sediment provenance, Lower Cretaceous Scotian Basin, eastern Canada. *Sediment. Geol.* **2011**, *237*, 150–165. [[CrossRef](#)]
61. Marsaglia, K.M.; DeVaughn, A.M.; James, D.E.; Marden, M. Provenance of fluvial terrace sediments within the Waipaoa sedimentary system and their importance to New Zealand source-to-sink studies. *Mar. Geol.* **2010**, *270*, 84–93. [[CrossRef](#)]

62. Rieser, A.B.; Liu, Y.; Genser, J.; Neubauer, F.; Handler, R.; Friedland, G.; Ge, X. $^{40}\text{Ar}/^{39}\text{Ar}$ ages of detrital white mica constrain the Cenozoic development of the intracontinental Qaidam Basin, China. *Geol. Soc. Am. Bull.* **2006**, *118*, 1522–1534. [[CrossRef](#)]
63. Hanson, A.D. *Organic Geochemistry and Petroleum Geology, Tectonics and Basin Analysis of Southern Tarim and Northern Qaidam Basins, Northwest China*; Stanford University: Stanford, CA, China, 1999.
64. Liu, B.J.; Ceng, Y.F. *Lithofacies Paleogeographic Basis and Working Methods*, 3rd ed.; Geological Publishing House: Beijing, China, 1985; pp. 1–442.
65. Boggs, J.S. *Petrology of Sedimentary Rocks*, 1st ed.; Cambridge University Press: Cambridge, UK, 2009; pp. 1–600.
66. Deer, W.A.; Howie, R.A.; Zussman, J. *An Introduction to the Rock-Forming Minerals*, 3rd ed.; Longman: London, UK, 2013; pp. 1–696.
67. Liu, L.; Chen, D.; Wang, C.; Zhang, C. Geochronology and structurology of HP–UHP rocks from the Altyn Tagh, northern Qaidam and Northern Qinling Mountains. *J. Northwest Univ. (Nat. Sci. Ed.)* **2009**, *39*, 472–479.
68. Liu, L.; Wang, C.; Chen, D.; Zhang, A.; Liou, J. Petrology and geochronology of HP–UHP rocks from the South Altyn Tagh, northwestern China. *J. Asian Earth Sci.* **2009**, *35*, 232–244. [[CrossRef](#)]
69. Wang, C.; Liu, L.; Yang, W.Q.; Zhu, X.H.; Cao, Y.T.; Kang, L.; Chen, S.F.; Li, R.S.; He, S.P. Provenance and ages of the Altyn Complex in Altyn Tagh: Implications for the early Neoproterozoic evolution of northwestern China. *Precambrian Res.* **2013**, *230*, 193–208. [[CrossRef](#)]
70. Ren, S.M.; Ge, X.H.; Liu, Y.J.; Ge, X.H.; Wu, G.D.; Yuan, S.H. Multi-stage strike-slip motion and uplift along the Altyn Tagh Fault since the Late Cretaceous. *Geol. Bull. China* **2004**, *23*, 926–932.
71. Wan, J.L.; Wang, Y.; Li, Q.; Wang, F.; Wang, E.Q. FT Evidence of Northern Altyn Uplift in Late-Cenozoic. *Bull. Mineral. Petrol. Geochem.* **2001**, *20*, 222–224.
72. Chen, Z.L.; Gong, H.L.; Li, L.; Wang, X.F.; Chen, B.L.; Chen, X.H. Uplift and exhumation of the Altyn Mountains during Neogene. *Earth Sci. Front.* **2006**, *13*, 91–102.
73. Fu, L. *Fine-Scale Division of the Paleogene–Neogene Sedimentary System in the Western Qaidam Basin and Its Implications for Tectonic Evolution*; Peking University: Beijing, China, 2015.
74. Sobel, E.R.; Arnaud, N.; Jolivet, M.; Ritts, B.D.; Brunel, M. Jurassic to Cenozoic exhumation history of the Altyn Tagh range, northwest China, constrained by $^{40}\text{Ar}/^{39}\text{Ar}$ and apatite fission track thermochronology. *Geol. Soc. Am. Mem.* **2001**, *194*, 247–267.
75. Li, H.B.; Yang, J.S.; Xu, Z.Q.; Sun, Z.M. Constraints of the Altyn Tagh Fault on the Growth and Uplift of the Northern Tibetan Plateau. *Earth Sci. Front.* **2006**, *13*, 59–79.

Disclaimer/Publisher’s Note: The statements, opinions and data contained in all publications are solely those of the individual author(s) and contributor(s) and not of MDPI and/or the editor(s). MDPI and/or the editor(s) disclaim responsibility for any injury to people or property resulting from any ideas, methods, instructions or products referred to in the content.